$\overline{u'v'}$ Reynolds Stress in the Viscous Sublayer over a Wide Range of *Re* Numbers

Christer Rosén and Christian Trägårdh
Division of Food Engineering, University of Lund, S-221 00 Lund, Sweden

To test the ability of different turbulence models to predict the turbulent momentum transport in the viscous sublayer, measurements are performed with a laser Doppler velocimeter (LDV). The main objective of the experiments is to measure the $\overline{u'v'}$ correlation in the near wall region. The results support the correlation: $-\overline{u'v'}^{+} = A_k y^{+3}$. The results of 2-D computer simulations using four different low Reynolds number k-ϵ turbulence models are compared with the experimental LDV data. The models tested are the original low Reynolds number k-ϵ model of Jones and Launder (1972, 1973) and three later modifications by Chien (1980), Lam and Bremhorst (1981), and Nagano and Hishida (1987). The $\overline{u'v'}$ correlation was found to be underestimated with all four models, but the Chien model was superior, with only a 40% underestimation in the viscous sublayer.

Introduction

If gradients in static pressure, temperature or concentration are small and if mass fluxes are small or absent, then near-wall mean and turbulence quantities vary in a known and predictable way from one flow situation to another. Thus, a measured distribution of the turbulent viscosity or measured mass- or heat-transfer coefficients from one set of data can be used to predict other flows which fulfill the above requirements. However, if any of these requirements is not fulfilled, then the "universality" is lost. A well-known example of such a situation is when heating or cooling creates sharp temperature gradients. Another example, which we have mainly dealt with (Rosén, 1992), is high Schmidt number ($1{,}000 < \sigma < 100{,}000$) mass transfer in the concentration boundary layer over ultrafiltration membranes.

Ultrafiltration is a pressure-driven membrane process and the membranes selectively retain macromolecules. The macromolecules filtered in UF have physical properties which are highly concentration-dependent, and the property gradients near the membrane surface become very steep. The viscosity "at" the membrane surface can be more than ten times higher than the bulk viscosity. To predict "nonuniversal" flows, such as flows exhibiting gradients of physical properties, injection or suction, a "model" is needed that can spatially resolve these phenomena. A numerical procedure which can solve the governing transport equations will be the required "model." When turbulent flows are considered, as here, a turbulence model is also required to calculate the turbulent transport of momentum. Various models can be used to calculate the Reynolds stresses, which have been a popular tool during the past 20 years. Extensive review articles have been written by, for example, Rodi (1980), Patel et al. (1985), Nallasamy (1987), and Hanjalic (1988). One of the most widely used group of models is the *k*-ϵ turbulence models which employ two transport equations: one for the turbulent kinetic energy and the other for the dissipation rate of turbulent kinetic energy. Despite the fact that this group of models is based on rather severe simplifications and assumptions (Rodi, 1980; Hanjalic, 1988), it still remains one of the most widely used approaches by scientists and engineers.

One of the main objectives of this work is to find a low Reynolds number *k*-ϵ turbulence model that predicts correctly in the viscous sublayer to calculate high Schmidt number mass transfer. The low molecular diffusivity of high Schmidt number ($1{,}000 < \sigma < 100{,}000$) solutes leads to a much thinner concentration boundary layer than the momentum boundary layer. The concentration boundary layer is only a few y^+ in thickness and does not extend beyond the viscous sublayer (Mizushina et al., 1971; Shaw and Hanratty, 1977). In this region, the turbulent transport of momentum is very small compared with the molecular transport of momentum. The magnitude of the turbulent viscosity below $y^+ = 2$ is less than 1% of the kinematic viscosity. However, for high-Schmidt-number mass transport,

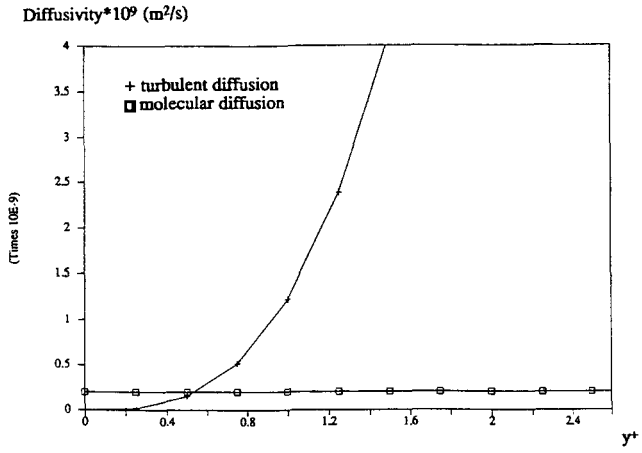

Figure 1. Molecular and turbulent diffusion for a solute with $\sigma = 5{,}000$ at $Re = 20{,}000$.

the situation is different, as shown in Figure 1 where the turbulent and molecular diffusions are compared for a solute with a Schmidt number of 5,000. In the calculations of mass transfer it is common to use a turbulent Schmidt number to relate the turbulent transport of momentum to the turbulent transport of a species concentration. So, to calculate high-Schmidt-number mass transport via the turbulent Schmidt number concept, accurate predictions must also be made in the viscous sublayer of the turbulent transport of momentum.

In this article, results from laser Doppler velocimeter (LDV) measurements are compared with simulation results from four different low Reynolds number k-ϵ models. Emphasis is placed on the performance of the models in the viscous sublayer.

Theories and Methods

Momentum transport

The time-averaged Navier Stokes equations, so-called Reynolds' equations, read in the Cartesian coordinate system, for a steady, two-dimensional boundary layer flow:

$$\overline{U}\frac{\partial(\rho\overline{U})}{\partial x}+\overline{V}\frac{\partial(\rho\overline{U})}{\partial y}=-\frac{\partial\overline{P}}{\partial x}+\frac{\partial}{\partial y}\left(\nu\frac{\partial(\rho\overline{U})}{\partial y}\right)-\frac{\partial}{\partial y}\left(\rho\overline{u'v'}\right) \quad (1)$$

Calculation of the $\overline{u'v'}$ correlation: Low-Reynolds-number k-ϵ models

To predict $\overline{u'v'}$, the turbulent eddy viscosity concept is used in this work:

$$-\overline{u'v'}\equiv\nu_t\frac{\partial\overline{U}}{\partial y} \quad (2)$$

Four low-Reynolds-number k-ϵ models, Chien, 1980 (CH), Jones and Launder, 1972, 1973 (JL), Lam and Bremhorst, 1981 (LB), Nagano and Hishida, 1987 (NH)] have been tested to calculate the eddy diffussivity ν_t with special consideration regarding its performance in the wall-near behavior of the viscous sublayer. The turbulent viscosity is for the k-ϵ models derived as:

$$\nu_t = C_\mu f_\mu \frac{k^2}{\tilde{\epsilon}} \quad (3)$$

where C_μ is a model parameter and f_μ is an empirical function.

The k-ϵ models employ two transport equations, one for the turbulent kinetic energy $k[k\equiv(1/2)(\overline{u_i'^2})]$ and the other for the turbulent kinetic energy dissipation rate $[\epsilon\equiv\nu(\partial u_i'/\partial x_j)/(\partial u_i'/\partial x_j)]$ from which the k and ϵ fields are calculated. The transport equations for k and ϵ read in the Cartesian coordinate system for a steady, two-dimensional, incompressible boundary layer flow:

$$\overline{U}\frac{\partial k}{\partial x}+\overline{V}\frac{\partial k}{\partial y}=\frac{\partial}{\partial y}\left[\left(\nu+\frac{\nu_t}{\sigma_k}\right)\frac{\partial k}{\partial y}\right]+\nu_t\left(\frac{\partial\overline{U}}{\partial y}\right)^2-\epsilon \quad (4)$$

$$\overline{U}\frac{\partial\tilde{\epsilon}}{\partial x}+\overline{V}\frac{\partial\tilde{\epsilon}}{\partial y}=\frac{\partial}{\partial y}\left[\left(\nu+\frac{\nu_t}{\sigma_\epsilon}\right)\frac{\partial\tilde{\epsilon}}{\partial y}\right]+C_{\epsilon1}f_1\frac{\tilde{\epsilon}}{k}\nu_t\left(\frac{\partial\overline{U}}{\partial y}\right)^2-C_{\epsilon2}f_2\frac{\tilde{\epsilon}^2}{k}+E \quad (5)$$

where

$$\epsilon=\tilde{\epsilon}+D$$

and $R_t\equiv k^2/\nu\tilde{\epsilon}$, $R_y\equiv\sqrt{k}y/\nu$, $y^+\equiv yu^*/\nu$.

In this set of equations, C_μ, $C_{1\epsilon}$, $C_{2\epsilon}$, σ_k, and σ_ϵ are constants also used in the high-Reynolds-number versions of the k-ϵ model. Their values are usually found by computer optimization. Table 1 shows low-Reynolds-number k-ϵ model parameters and functions.

Numerical method

The numerical method used to solve the transport equations for U, V, k and ϵ is a control volume formulation and is detailed by Patankar (1980). An adapted and modified form of the computer code PASSABLE was employed in the simulation program used in the work. PASSABLE is a code for boundary layer and other parabolic flows. It solves an equation of the type:

$$\overline{U}\frac{\partial(\rho\phi)}{\partial x}+\overline{V}\frac{\partial(\rho\phi)}{\partial y}=\frac{\partial}{\partial y}\left[\Gamma\frac{\partial(\rho\phi)}{\partial y}\right]+S \quad (6)$$

in a step-by-step forward marching procedure. Here, ϕ denotes the dependent variable ($\overline{U}$, $\overline{V}$, k and ϵ), Γ is the corresponding diffusion coefficient, and S is a source/sink term. Only the variables of the step under considerations and those from the previous step are stored. The fields of the dependent variables are given initial values, and the stepwise procedure is thereafter maintained until a convergent solution is obtained.

The number of nodal points used was between 120-200, and the first point was situated at $y^+\approx0.001-0.01$. To obtain sufficient resolution in the near wall region, the nodal points were placed closer and closer as the wall was approached. Somewhat less than half of the nodal points were situated below $y^+=5$. The simulation results were found to be independent

Table 1. Low-Reynolds-Number k-ϵ Model Parameters and Functions: $\sigma_k = 1.0$ and $\sigma_\epsilon = 1.3$

Code	$C_{\epsilon 1}$	$C_{\epsilon 2}$	C_μ	E	D	$\tilde{\epsilon}_w$	f_μ	f_1	f_2
JL	1.55	2.00	0.09	$2\nu\nu_t\left(\frac{\partial^2\overline{U}}{\partial y^2}\right)^2$	$2\nu\left(\frac{\partial\sqrt{k}}{\partial y}\right)^2$	0	$e^{-2.5/(1+R\sqrt{50})}$	1.0	$1-0.3e^{-R_t^2}$
CH	1.35	1.8	0.09	$-2\nu\frac{\tilde{\epsilon}}{y^2}e^{-0.5y^+}$	$2\nu\frac{k}{y^2}$		0 $1-e^{-c_3y^+}$ where $c_3=0.0115$	1.0	$1-0.22e^{-(R\sqrt{6})^2}$
LB	1.44	1.92	0.09	0	0	$\nu\frac{\partial^2 k}{\partial y^2}$	$(1+20.5/R_t)\times(1-e^{(-0.0165R_y)})^2$	$1+(0.05/f_\mu)^3$	$1-e^{(-R_t^2)}$
NH	1.45	1.9	0.09	$(1-f_\mu)\nu\nu_t\left(\frac{\partial^2\overline{U}}{\partial y^2}\right)^2$	$2\nu\left(\frac{\partial\sqrt{k}}{\partial y}\right)^2$	0	$(1-e^{-y^+/26.5})^2$	1.0	$1-0.3e^{-R_t^2}$

of the number of nodal points and of the initial values of the fields of the dependent variables.

Measurements of the $\overline{u'v'}$ correlation: experimental setup

The experiments were carried out in a 3.5-m-long rectangular channel (0.14×0.05 m^2). The mean flow in the circuit was measured with an electromagnetic flowmeter. Measurements were made with the LDV measuring device through a window 0.4 m from the outlet (see Figure 2). The low aspect ratio of the channel was chosen as a practical necessity. It would have been desirable to have a higher aspect ratio so that three-dimensional effects could have been avoided. Measurements over ultrafiltration membranes were performed in the same equipment (Rosén, 1992), and because of the relatively high pressures used in the ultrafiltration experiments it was not possible to increase the dimensions of the channel.

Measurements of the $\overline{u'v'}$ correlation: LDV system

A TSI system 9100-7 with two blue beams and two green beams was used: two velocity components were measured simultaneously, one with each color. The conventional beam configuration was rearranged so that measurements could be made closer to the surface. The four beams are usually situated symmetrically around a central point. In the setup, the beam in the lowest position was raised to the central position so that the beams measuring the horizontal flow component and one of the other two beams were at the same level (see Figure 2). This setup was chosen because of the desire to measure as close as possible to the wall. To avoid the beams striking the lower surface of the channel before the measuring point was reached, the channel was tilted at an angle of 3°. Due to this and the fact that the beam in the lowest position is raised to a central position, the velocity component perpendicular to the lower surface was rotated by an angle of 6°. Tilting of the channel in relation to the optical axis and rotation of the green beam pair for the V velocity measurement cause an angular deviation from orthogonality as pointed out by Karlsson et al. (1992). The difference between measured velocity and velocity in the normal direction was about 0.5%. With this beam configuration and a lens of 120 mm in focal length and beam expansion to reduce the probe volume size, a measuring volume with a height of 20 μm and length of 100 μm would be created ideally. Compare the size of the measuring volume with the viscous lengths in Table 2 for an impression of its relative size. Backscattered light collection was employed. Silicone carbide seeding (mean diameter 1.5 μm) was added to the fluid to increase the data generation rate.

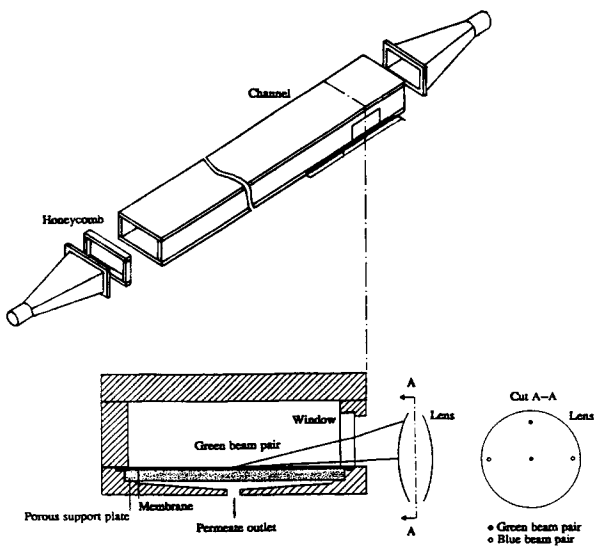

Figure 2. Cross-section of the channel.

The green beam pair used to measure the velocity component normal to the surface is arranged for near-wall measurements.

The main objective was to obtain measurements of the Reynolds stress $-\rho\overline{u'v'}$ close to the wall. To attain this the measuring volumes for both beam colors must coincide. The difference in the optical pathways of the two pairs of beams gives rise to a difference in the locations of the two measuring volumes. These were made to coincide by using the beam steering capability of the LDV device. The positions of the measuring volumes were checked by traversing one beam at a

Table 2. Scales and Parameters for Cases A, B and C

Case	$\overline{U}$ m/s	Re	u^* mm/s	t^* ms	l^* μm
A	0.106	7,800	7.07	20.0	127.0
B	0.211	8,500	14.28	8.7	118.0
C	0.276	20,000	14.95	4.9	63.0

time, in steps of 10 μm, past a fixed set of cross wires (diameter 5 μm) situated in the channel at the measuring point. The edges of the beams could thus be found by observing the cross wires (when one of the wires was hit by the beam, a sharp reflection was seen from the wire). With this technique and with measurements from the unstirred initial "TSI setup," the shape and size of the measuring volumes found were roughly the same as those predicted by theoretical calculations (Johansson, 1988b). The theoretically expected displacement between the two measuring volumes in the direction of the optical axis, due to the asymmetrical beam configuration, was also observed.

This choice of optical setup and beam steering does not lead to the ideal case, with the beams crossing at the beam waists, which is assumed when calculating the velocity from the Doppler shift of the frequency. However, since the shape of the beams near the beam waists changes very slowly, only small errors occur in the results when the distance from the measuring point to the beam waist is reasonably small. The calculated error was $<1\%$ (Hanson, 1973).

To measure correctly the Reynolds stress, the measurements of the two components must coincide not only in space but also in time. Therefore, a coincidence window was set at the counter of the LDV device. This is a time interval, τ_c, during which measurements of both components must be generated to be accepted as valid data. This interval is dictated by the maximum and minimum time required for the two velocity components to generate a valid sample.

Measurements of the $\overline{u'v'}$ correlation: data collection routine

A problem of using the LDV technique is that it is not possible to choose the time interval for velocity measurements. To minimize bias effects due to velocity-dependent sampling rates, data on a time scale shorter than a characteristic time scale of the flow have been collected. A measure of the shortest time scale is the viscous time $t^*[=\nu/(u^*)^2]$. If the time interval between the measurements can be kept below t^*, a quasi continuous time series will be obtained. For this reason, the flow was heavily seeded and the counters in the LDV system were set to work in the continuous mode. The information on the elapsed time between data points was collected and used in the calculation of turbulence statistics to give proper weight to each individual sample.

Below $y^+=5$, it became difficult to maintain the data collection rate. More than 60,000 values were collected at each measuring point to obtain high accuracy in the calculations of the turbulent statistics. Below $y^+=5$, fewer data were collected because of lower data generation rates. The counters have validation circuitry which should exclude incorrect measurements. However, some bad samples were still accepted, which have been removed by the following routine. The data set was searched for the lowest and highest velocities. Thereafter, the interval between them was divided into 100 equally large "boxes" and each data point was sorted into the appropriate "box." If in the ten highest and/or lowest intervals there were one or two data points, the most extreme data point was removed. This procedure was repeated until no outliers were found. The number of bad samples increased as the wall was approached, but was never more than 0.1% of the total number of data points. The data-collecting routine described here is the same as that used by Johansson (1988b). In his thesis, Johansson shows that it is possible to obtain virtually continuous time histories of the velocity components in a turbulent flow field using this technique in a counterbased LDV system.

Measurements of the $\overline{u'v'}$ correlation: experimental test cases

Results are reported from three cases:

(A) Water and small amounts of Dextran T70 (0.125 wt. %), $u_m=0.106$ m/s; hydraulically smooth channel

(B) Glycerol-water mixture (25 wt. % glycerol) into which 0.125 wt. % Dextran T70 was added, $u_m=0.211$ m/s; the viscosity of this mixture was 1.95 times the viscosity of water; hydraulically smooth channel

(C) Water and small amounts of Dextran T70 (0.125 wt. %), $u_m=0.276$ m/s; hydraulically smooth channel; maximum 20,000 data values

Results: LDV Measurements

Mean velocity profile

Mean velocity profiles could be measured down to $y^+\simeq 0.6$, $(y^+=yu^*/\nu)$, in cases A and B and in case C down to $y^+\simeq 2.3$. The fit to the linear profile below $y^+=5$ is good. Linear regression gives a standard error of the coefficient of direction that is less than 1%. The friction velocity u^* is a key factor in scaling accuracy. Considering the small error in the coefficient of direction, temperature variance in the circuit and the fact that velocity bias cannot be excluded in the near wall region (since the data generation rate is decreased), the error in u^* was estimated to have a standard deviation in the range 2–5%. It was not possible to measure closer to the wall, mainly because of poor signal quality caused by flare from the wall. One difficulty with LDV measurements is the determination of the exact position of the wall. The "zero-level" experimentally obtained was corrected by extrapolating the linear velocity profile below $y^+=5$ to pass through the origin. Since the standard error of the coefficient of direction was low, $<1\%$, the estimate is that the error in y was in the range 0.005–0.01 mm. This corresponds to y^+ values in the range $0.05\text{–}0.1y^+$. The friction velocities in Table 2 were calculated from the velocity gradients below $y^+=5$.

Turbulence intensities and higher-order moments

To check the quality of the measurements of turbulence intensities, skewness and flatness factors were calculated for the two velocity components. Good agreement was found with literature values, but a decrease in quality for the V component was found in the third and fourth moments. This decrease was probably due to strong flare from the upper green beam as it hits the wall.

In Figure 3 the local turbulence intensities for the velocity component in the mean flow direction U, $(=\sqrt{\overline{u'^2}}/\overline{U})$, and the velocity component V, $(=\sqrt{\overline{v'^2}}/\overline{U})$, are shown. There is good agreement with measured turbulence intensity profiles reported in the literature (for example, Johansson, 1988a,b; Nishino and Kasagi, 1989). A value of about one of the skewness factor was obtained in the near-wall region, for the main

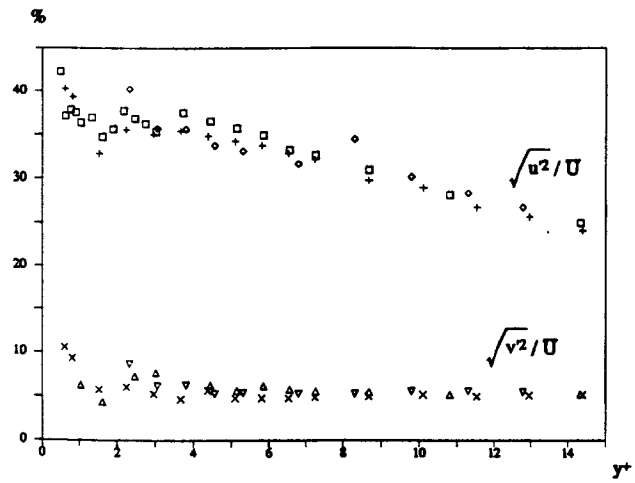

Figure 3. Local turbulence intensities in inner-law scaling.

□, Δ, $Re = 7{,}800$; +, ×, $Re = 8{,}500$; ◇, ▽, $Re = 20{,}000$.

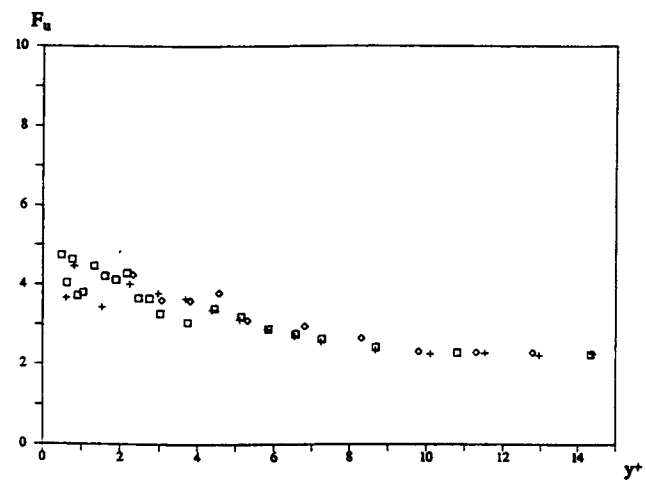

Figure 5. Flatness factor for *U*.

□, $Re = 7{,}800$; +, $Re = 8{,}500$; and $Re = 20{,}000$.

flow direction component $S_u[=\overline{u'^3}/(\sqrt{\overline{u'^2}})^3]$ shown in Figure 4, which is the same as reported by others (Johansson, 1988a,b; Nishino and Kasagi, 1989). At about $y^+ = 12$, a change in sign, from positive to negative, is reported in the literature which was also found in these measurements. The skewness factor $S_v[=\overline{v'^3}/(\sqrt{\overline{u'^2}})^3]$ in Figure 4 is essentially in agreement with reported results down to about $y^+ = 2$, but below $y^+ = 2$ a different trend was observed in the measurements. Instead of attaining positive values, the curves turn downward to negative values. This decrease in quality is revealed in the sensitive third moment. As the difference is not large compared with other measurements, this quality decrease is probably not of any major importance when calculating moments of lower order or in the calculation of the Reynolds stress $-\rho\overline{u'v'}$. A value of the flatness factors of U in Figure 5, $[F_u = \overline{u'^4}/(\sqrt{\overline{u'^2}})^4]$, of about 4.2 in the near-wall region has been reported in the literature which also was found in these measurements. The flatness factor F_v for $y^+ < 20$ is in the range between 4 and 15 as expected, but the data scattered to a high degree as shown in Figure 6 and is mainly attributed to the high noise level due to flare from the wall. Another contributing factor to this scatter is the case of collecting a too low number of data values. This number was chosen to give a stable third moment which guarantees correct values of this and lower moments (as the $\overline{u'v'}$ correlation).

Reynolds shear stress

In Figures 7a-7c, the experimental results are shown for cases A, B and C, respectively, of the variation of $-\overline{u'v'}$ in the viscous sublayer. In Figure 8, the measured variation of $-\overline{u'v'}$ for case B is extended to higher y^+ values. Figure 8 shows that a value of about 0.5 at $y^+ = 12$ was found, as expected.

The skewness and flatness factors have been calculated from the LDV measurements of $u'v'$, as shown in Figures 9 and 10. Good agreement was found with those of Johansson (1988a,b).

The following equation can be derived from a Taylor series expansion of the turbulence shear stress $-\overline{u'v'}^+$, for $y^+ \to 0$

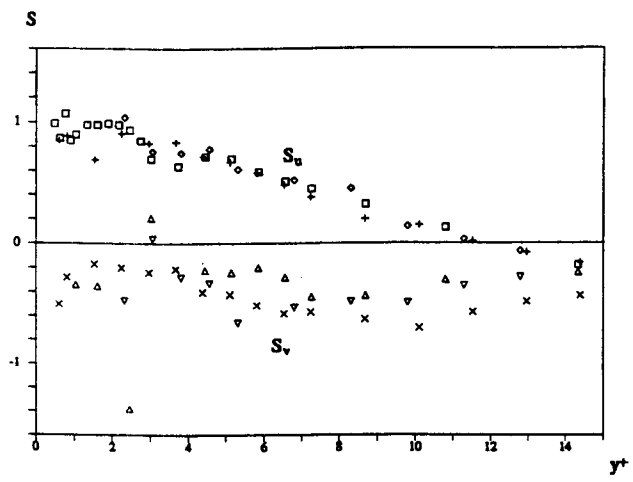

Figure 4. Skewness factors for *U* and *V*.

□, Δ, $Re = 7{,}800$; +, × $Re = 8{,}500$; ◇, ▽ $Re = 20{,}000$.

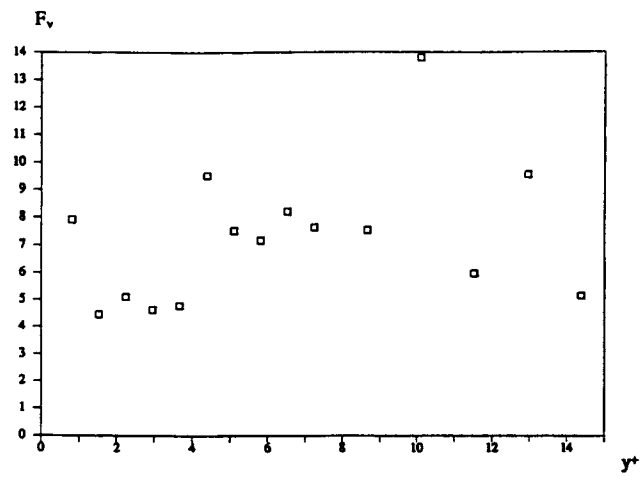

Figure 6. Flatness factor for *V*: case B.

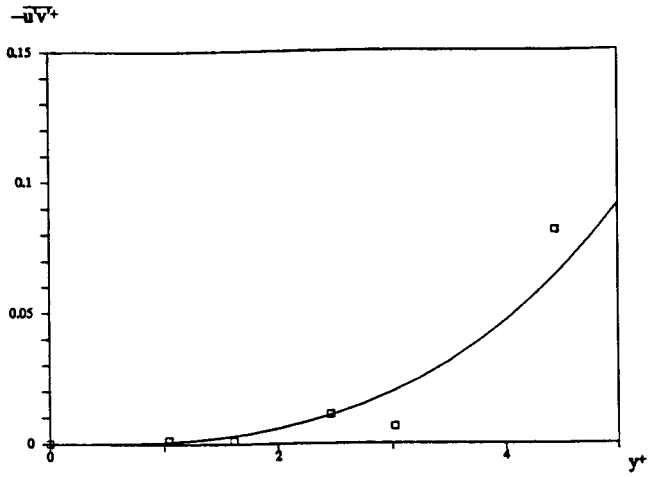

Figure 7a. Dimensionless Reynolds stress, $-\overline{u'v'}/u^{*2}$ vs. y^+: case A.

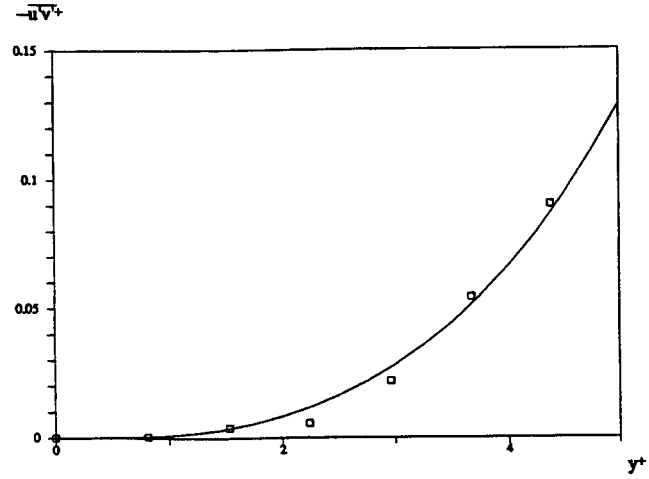

Figure 7b. Dimensionless Reynolds stress, $-\overline{u'v'}/u^{*2}$ vs. y^+: case B.

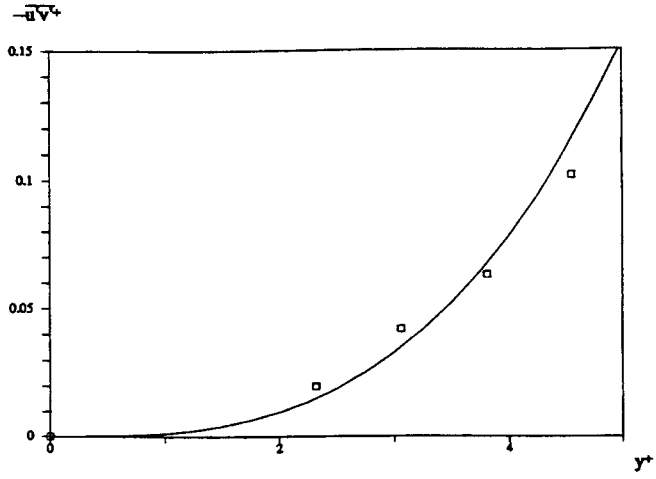

Figure 7c. Dimensionless Reynolds stress, $-\overline{u'v'}/u^{*2}$ vs. y^+: case C.

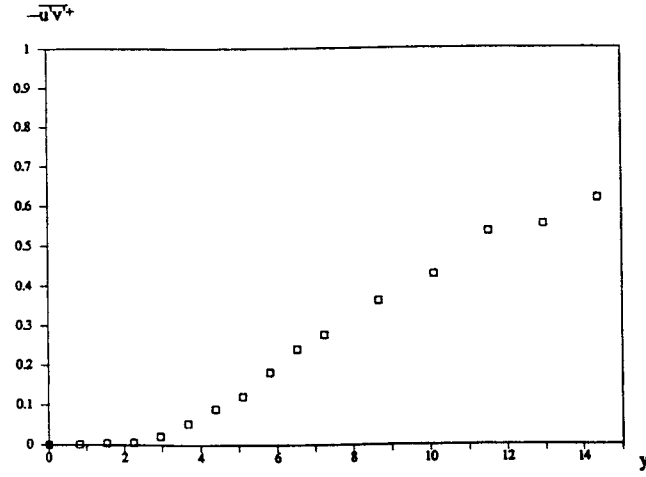

Figure 8. Dimensionless Reynolds stress, $-\overline{u'v'}/u^{*2}$ vs. y^+, extended to higher y^+ values: case B.

(for example, Hinze, 1959, p. 620; Monin and Yaglom, 1975, p. 279):

$$-\overline{u'v'}^+ = Ay^{+3} + By^{+4} + \ldots \tag{7}$$

If y^+ is small the variation in $\overline{u'v'}^+$ can be expressed by the leading term in Eq. 7:

$$-\overline{u'v'}^+ = A_1 y^{+n} \tag{8}$$

To decide the power of the correlation fits were made of the experimental results to the following rewritten form of Eq. 8:

$$\log\left(-\overline{u'v'}^+\right) = \log\left(A_1\right) + n \log\left(y^+\right) \tag{9}$$

Plotting $\log\left(-\overline{u'v'}^+\right)$ vs. $\log(y^+)$ gives a line whose slope is n. In Table 3, results are presented for n. Results are also included from other near-wall measurements; LDV measurements by Johansson and Karlsson (1988a) and measurements performed by Nishino and Kasagi (1989) with a three-dimen-

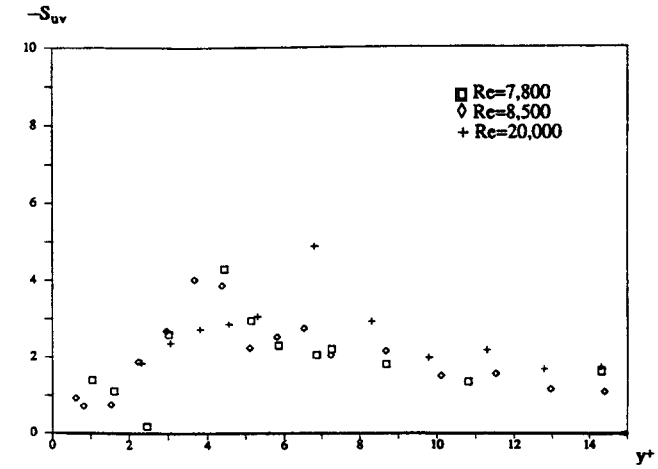

Figure 9. Skewness factor for the Reynolds stress.

□, $Re = 7{,}800$; ◇, $Re = 8{,}500$; +, $Re = 20{,}000$.

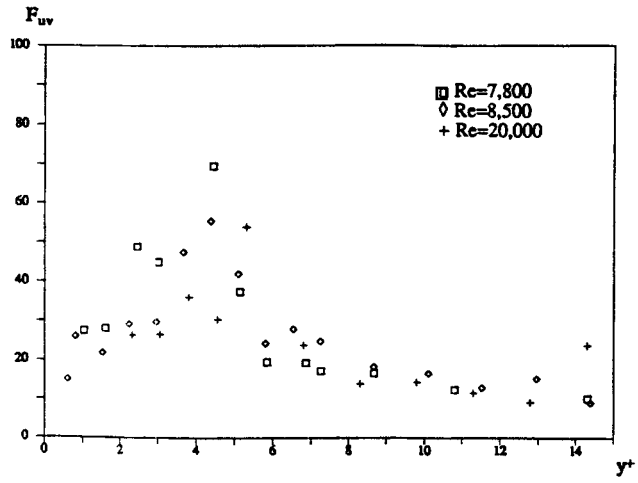

Figure 10. Flatness factor for the Reynolds stress.

□, $Re = 7{,}800$; ◇, $Re = 8{,}500$; +, $Re = 20{,}000$.

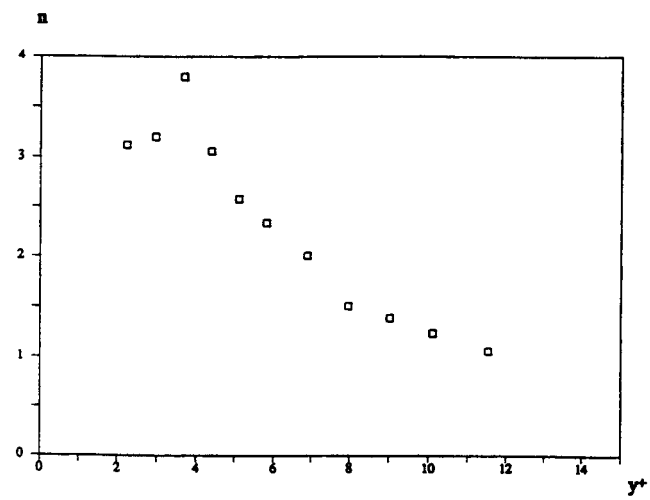

Figure 11. Exponent *n* plotted against a midpoint value of y^+ for different intervals of y^+.

sional particle-tracking velocimeter. Results are also given from low-Reynolds-number direct numerical simulations of the Navier-Stokes equations (Kim et al., 1987). The experimental results support the correlation, $-\overline{u'v'}^+ = A_1 y^{+3}$, although the experimental uncertainty in this region is quite high. The fits of the data to the y^{+3} correlation are rather good at low Reynolds numbers. The fit of the results from the direct numerical simulations is, in fact, almost perfect. However, for high Reynolds numbers the fits are poorer. This discrepancy can be explained by the fact that the region over which the y^{+3} expression is valid moves closer to the wall with increasing Reynolds number, while the closest measuring point in dimensionless units is further from the wall. In Figure 11, the exponent n in Eq. 15 is shown from fits of the experimental data of case B. The point with the lowest y^+ value is obtained for the five measuring points closest to the wall, the next fit in the diagram is for the measuring points 2 to 6 and so on. The y^+ values are for the middle of each y^+ interval. The value for the n exponent decreases with increasing y^+ value. The reason for the difference in the value of the exponent might also be that the experimental error in the determination of the dimensionless distance is increased when the Reynolds number is increased. The physical distance in meters corresponding to a dimensionless distance unit is decreased with increasing Reynolds number (since the friction velocity increases), while the experimental errors corresponding to the determination of the physical distance from the wall are of the same magnitude.

Fits has also been made to a pure y^{+3} correlation:

$$-\overline{u'v'}^+ = A_k y^{+3} \tag{10}$$

Table 3. Results from Fits to Eq. 16

Results from	*Re*	$n \pm SD$ Error ($y^+ < 4$)
Kim et al. (1987)	5,700	3.01 ± 0.01
Nishino et al. (1989)	6,560	2.58 ± 0.07
Rosén (1992)	7,800	3.02 ± 0.48
Rosén (1992)	8,500	3.11 ± 0.31
Rosén (1992)	20,000	2.31 ± 0.20
Johansson et al. (1988)	75,600	2.32 ± 0.16

A comparison between the experimental data points and the obtained y^{+3} correlations (the solid lines) is made in Figure 7. In Figure 12, the results of A_k coefficients are compared. These coefficients are obtained from least-squares fits of experimental results to y^{+3} correlations according to Eq. 10. There is a clear tendency toward increasing A_k with increasing Reynolds number. The Reynolds number from the measurements of this article and those of Johansson and Karlsson is based on the hydraulic diameter due to low aspect ratios, while in other cases it is based on the half-channel height due to high aspect ratios (>10). The obtained values of A_k can be described as a function of the Reynolds number:

$$A_k = 0.0014[1 - \exp(-\sqrt{Re_{mod}}/2)] \tag{11}$$

where $Re_{mod} \equiv (Re - 3{,}000) \times 10^{-3}$.

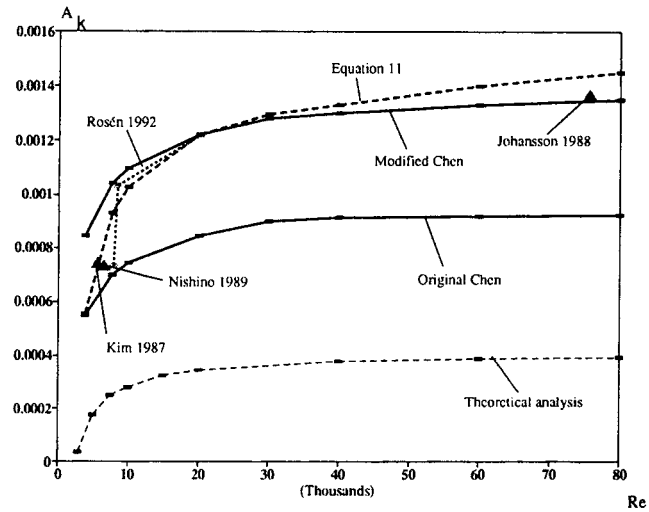

Figure 12. Measured, simulated and theoretically derived A_k as influenced by the Reynolds number.

Influence of Reynolds number on the $\overline{u'v'}$ correlation coefficient A_k: theoretical analysis

The influence of the Reynolds number on A_k can be explained from theoretical considerations. The following equation is valid for a fully developed flow (Tennekes and Lumley, 1972):

$$1-\frac{2y^+}{h^+}=\frac{du^+}{dy^+}-\overline{u'v'}^+ \tag{12}$$

where h^+ is the dimensionless height of the channel. If Eq. 10 is adopted, then A_k can be expressed as:

$$A_k=\left(1-\frac{2y^+}{h^+}-\frac{du^+}{dy^+}\right)\Big/y^{+3} \tag{13}$$

The variation of the dimensionless velocity u^+ ($=\overline{U}/u^*$) across a constant-stress inner layer is constrained by the following expressions as boundary conditions:

$$u^+=0 \text{ and } \overline{u'v'}^+=0 \text{ at } y^+=0 \tag{14a}$$

$$u^+=(1/\kappa)\ln y^+ + B \text{ for } y^+>30\text{–}50 \tag{14b}$$

The restriction in Eq. 14a is a result of the "no-slip" condition, and Eq. 14b results from near-wall scaling and the assumption that the outer velocity defect law and inner wall law overlap in some region. A great deal of effort has been devoted to the construction of a single equation for u^+ in terms of y^+. These attempts were unsuccessful until Spalding (1961) observed that the inverse function could be obtained. Spalding proposed the following equation for $y^+=y^+(u^+)$ after considering the limiting conditions, together with experimental data:

$$y^+=u^+ + \exp(-A)\left[\exp(\kappa u^+)-1-\sum_{n=3}^{n=4}(\kappa u^+)^n/n!\right] \tag{15}$$

where $A=\kappa B$. The values, $\kappa=0.41$ and $B=5.2$, were adopted for this equation (usually reported values of B are about 5.0–5.5). Differentiation of Eq. 15 with respect to u^+ gives an expression for dy^+/du^+. After combining the expression for dy^+/du^+ with Eq. 13, the following relationship is obtained:

$$A_k=\left[1-\frac{2y^+}{h^+}-1\Big/\left\{1+\kappa\exp(-A)\left[\exp(\kappa u^+)-1-\sum_{n=1}^{n=3}(\kappa u^+)^n/n!\right]\right\}\right]\Big/y^{+3} \tag{16}$$

To calculate A_k, an expression is needed to describe $h^+(=hu^*/\nu)$. Dean (1978) made a comprehensive literature review of the Reynolds number influence on the friction factor for turbulent flow between parallel plates and suggested the following relationship:

$$f=0.073Re^{-0.25} \tag{17}$$

Due to the definitions of the friction factor and the friction velocity, the following equation is obtained for the dimensionless height:

$$h^+=0.191Re^{0.875} \tag{18}$$

If Eq. 18 is substituted into Eq. 16, then an expression is obtained from which A_k can be computed as a function of the Reynolds number using Eqs. 15, 16 and 18 at $y^+=5$ shown in Figure 12. The curve in Figure 12 has the same form as the experimentally obtained curve. The calculated A_k values are in good agreement, but the same level is not obtained. This difference might occur because of an overestimation of du^+/dy^+ and/or because the y^{+3} correlation is not valid as far out from the wall as $y^+=5$.

Table 4. Fanning Factor Predicted by k-ϵ Models and Dean's Correlation

Reynolds Number	Fanning Friction Factor				
	Dean	NH	LB	JL	CH
8,700	0.0078	0.0068	0.0066	0.0064	0.0067
22,600	0.0061	0.0054	0.0054	0.0052	0.0054

Computer Simulations

Mean velocity profile and friction factor

Simulations have been performed with all the models for fully developed turbulent flow between parallel plates. The expected $y^+\simeq u^+$ relationship was observed for all four models. Dean (1978) made a very comprehensive literature review of the influence of the Reynolds number on the friction factor and other bulk variables in two-dimensional rectangular duct flow of large aspect ratios. The computed values of the Fanning friction factor f are compared in Table 4 with Dean's suggested correlations for this quantity (see Eq. 17). As can be seen, an underestimation results with all models (in the order of 10%). This trend is also observed when a comparison is made with results from direct numerical simulations of the Navier-Stokes equations (Kim et al., 1987). (The predictions of the direct numerical simulations are quite close to the value obtained from Dean's correlation with only a ~3% underestimation.) The reason for the underestimation of the friction factor can probably be found in the procedure of tuning the model constants. Chien, for instance, tuned the constants against measurements of Laufer (1951), Clark (1968), Eckelman (1974), and Kreplin and Eckelman (1979). These experimental investigations report on spatially resolved measurements of turbulence statistics. The obtained f values in these experiments are about 10% lower than the values obtained from the correlation of Dean.

Reynolds shear stress

Simulation results of the Reynolds stress $-\rho\overline{u'v'}$ in the near-wall region showed large variations among the models. As can be seen in Figure 13, the calculated Reynolds stress is smaller than the experimentally found values in the near-wall region. The values obtained from the JL, LB and NH models are several orders of magnitude too small. The model of Chien shows superior behavior compared with the other models in

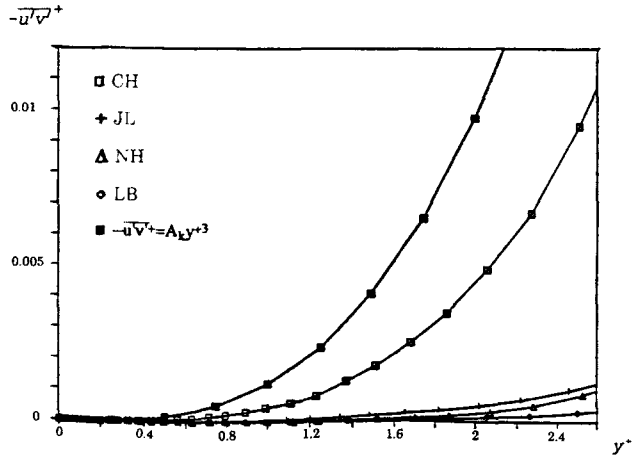

Figure 13. Dimensionless Reynolds stress, $\overline{u'v'}^+$ vs. y^+: $Re = 22{,}600$.

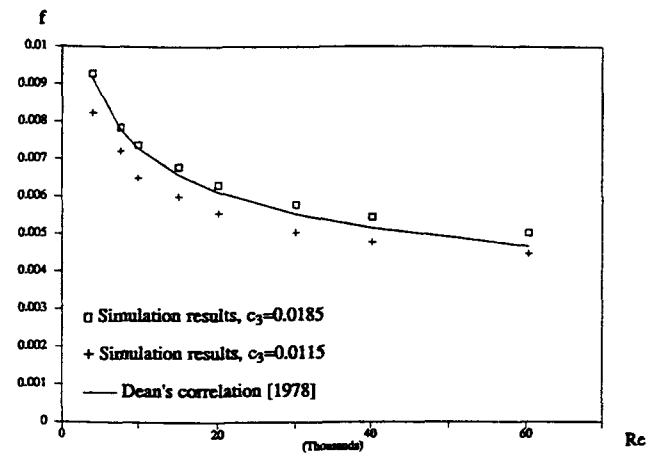

Figure 14. Fanning friction vs. the Reynolds number.

this respect, and an approximately 40% underestimation is observed for Reynolds numbers larger than 10,000. For smaller Reynolds numbers the underestimation is smaller. Simulation results from the Chien model and experimental values of A_k are shown in Figure 12.

Modification of the Chien model for the prediction of turbulent flow between parallel plates

As the Chien model had the closest agreement with measured data in the very near wall region of the viscous sublayer of $\overline{u'v'}$, it was chosen as the best alternative for further refinement so to fit the purpose here defined. (There is no major differences between the models in their ability to predict the law of the wall or other transport properties which distorted this choice.) Thus, to improve the performance of the Chien model a change was made in one of the model parameters. The value of c_3 in expression for f_μ (see Table 1) was changed to 0.0185. The choice for tuning this model parameter is based on the fact that it is contained in the wall damping function for the eddy viscosity expression.

The result was an increase in the predicted values of the Reynolds stress in the viscous sublayer. Simulation results of the Reynolds stress variation in the viscous sublayer with this modified Chien model are shown in Figure 12. Good agreement between simulation and experimental results was obtained concerning the effect of the Reynolds number on the values of A_k.

The computed values of the friction factor f obtained with the modified Chien model show better agreement with Dean's (1978) suggested correlation of this quantity at low or moderate Reynolds number, but become worse as the Reynolds number increases. There is an increased ability of the modified Chien model to predict the mean centerline velocity compared with a suggested correlation made by Dean (1978). Equation 17 is the relationship for f, and the centerline velocity is described by (see Figures 14 and 15):

$$u_c/u_m = 1.28Re^{-0.0116}$$

The prediction of ϵ is only slightly influenced by the modification of the expression for f_μ. The calculation of k^+ in the viscous sublayer follows almost precisely the equation proposed by Coles (1978); $k^+ = 0.05 \times y^{+2}$, but there is a decreased ability to calculate the expected peak value of k^+ at $y^+ \simeq 12$. The predicted peak value of the turbulent kinetic energy is decreased by $\sim 12.5\%$, which gives poorer agreement with experimental data. However, the predictions of the modified Chien model are not poorer than the predictions made by the other three models.

To test the ability of the modified Chien model to predict other flow geometries than flow between parallel plates, simulations were also performed of circular duct flow and flow over a flat plate with no pressure gradient. The results for flat plate flow were compared with experimental values obtained by Wieghardt and Tillmann (1951). The prediction of the friction factor is excellent with the original Chien model with only a 1% underestimation after 5 m, while the modified version overestimates the friction factor by 6.6%. Patel et al. (1985) who tested seven low Reynolds number k-ϵ models also made comparisons with Wieghardt and Tillman's experimental results. The best results were obtained with the Chien model, which gave a 1.2% overestimation. The results from the other models scattered significantly, and the second best model made a 7.8% miscalculation. So, the modified Chien model still

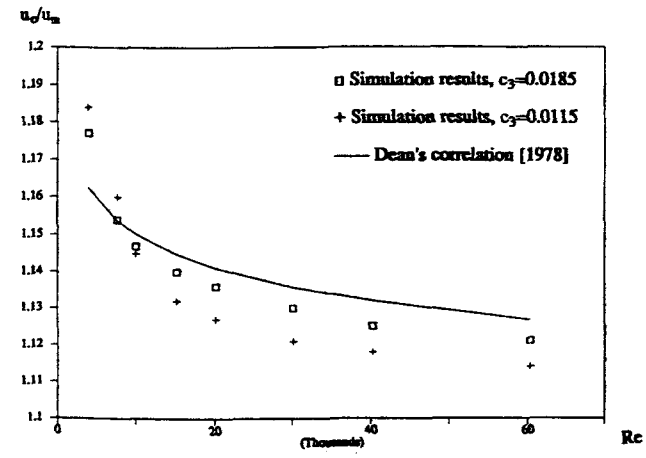

Figure 15. u_c/u_m vs. the Reynolds number.

makes better predictions than the other six low-Reynolds-number k-ϵ models (among others, LB and JL) tested by Patel et al. The simulated values of circular duct flow were compared with calculated values from the Blausius equation: $f=0.079Re^{-0.25}$. The agreement is good for the original Chien model, while the modified version gives an approximately 10% overestimation.

Finally, it must be pointed out that the modification made to the Chien model did not improve the model itself. It is merely a tuning of the constants in the model to predict turbulent flow between parallel plates with better accuracy. There are other means of obtaining this effect, but it is beyond the scope of this article.

Discussion

The most important results from the LDV measurements are the Reynolds stress profiles. Turbulence statistics show that the measurements are of high quality. The experimental results support the correlation, $-\overline{u'v'}^{+}=A_k y^{+3}$, in the viscous sublayer, although the experimental uncertainty is high. The fit was rather good at low Reynolds numbers, but worse at higher ones. A comparison with results found in the literature shows a clear trend of Reynolds number dependence on A_k. Due to the dependence of the Reynolds number on A_k, the classical idea of inner-law scaling is not valid for the Reynolds stress considered in the Reynolds number range covered. Recently, Wei and Willmarth (1989) published results of Reynolds number dependence on statistical turbulence quantities ($\overline{u'^2}$, $\overline{v'^2}$, and $\overline{u'v'}$). The results of this investigation also demonstrated that inner-law scaling is not valid in the Reynolds number range $3{,}000<Re<40{,}000$.

The transport equations for momentum were solved with the aid of a turbulence model. The turbulence model family chosen was low-Reynolds-number k-ϵ models. The four k-ϵ models tested described the velocity profile in the viscous sublayer for turbulent flow between parallel plates with fairly good accuracy. However, regarding the calculation of the Reynolds stress $-\rho\overline{u'v'}$, a comparison with the LDV results showed that the models underestimated the Reynolds stress in the viscous sublayer. The best fit to the experimental data was exhibited by the Chien model (1980) which gave calculated values of about 60% of the experimentally obtained values. The reason for this underestimation can probably be found in the criteria used for the optimization of simulation results of momentum, k, ϵ and overall parameters such as the friction factor. Since the molecular diffusivity in the calculation of these quantities in the viscous sublayer is several orders of magnitude greater than the turbulent diffusion, a miscalculation of $-\overline{u'v'}$ can be neglected for these quantities.

A numerical procedure spatially resolving the variables of the governing equations is very powerful for simulating transport phenomena, especially in more complex situation where the molecular properties like viscosity and diffusivity change due to local temperature or concentration gradients. A prerequisite is naturally that the model and procedure are reliable, especially in those regions where this is required, such as the case of high-Schmidt-number mass transfer very close to the wall ($y^+<1$) demonstrated in Figure 1. We have shown that this is possible and have made careful measurements to improve and validate a predictive model.

Acknowledgment

This work was supported by the Technical Research Council and the Swedish National Board for Industrial and Technical Development. The PASSABLE code was kindly supplied by Dr. M. A. Leschziner, University of Manchester Institute of Technology.

Notation

A, B, C = coefficients in the expression for the variation of $\overline{u'v'}$
A_k = coefficient in the correlation: $\overline{u'v'}^{+}=A_k y^{+3}$
A_1 = coefficient in the correlation: $\overline{u'v'}^{+}=A_1 y^{+n}$
B = constant in the logarithmic velocity law
C_μ = coefficient in the k-ϵ model
$C_{\epsilon 1}$ = coefficient in the k-ϵ model
$C_{\epsilon 2}$ = coefficient in the k-ϵ model
$\mathfrak{D}$ = molecular diffusivity, m^2/s
D = function in the k-ϵ model for low-Reynolds-number effects
E = function in k-ϵ model for low-Reynolds-number effect
f = Fanning friction factor
f_1 = function in the k-ϵ model
f_2 = function in the k-ϵ model
f_μ = wall-damping function in the k-ϵ model
F = flatness factor
h = height of channel (wall to wall), m
h^+ = dimensionless height of channel, $h^+=hu^*/\nu$
k = turbulent kinetic energy, m^2/s^2
k^+ = dimensionless turbulent kinetic energy, $k^+=k/(u^*)^2$
l^* = viscous length, $l^*=\nu/u^*$, m
n = exponent in Eq. 7
$\overline{P}$ = mean temporal pressure, N/m^2
Re = Reynolds number
Re_{mod} = $(Re-3{,}000)\times 10^{-3}$
R_t = turbulence Reynolds number, $R_t=k^2/\nu\epsilon$
R_y = turbulence Reynolds number, $R_y=\sqrt{k}y/\nu$
S = skewness factor; source term
t^* = viscous time, $t^*=\nu/(u^*)^2$, s
u^* = friction velocity, m/s
u' = fluctuating velocity in x direction, Cartesian coordinates, m/s
u_c = mean centerline velocity, m/s
u_m = mean bulk velocity, m/s
$\overline{U}$ = mean velocity in x direction, Cartesian coordinates, m/s
v = fluctuating velocity in y direction, Cartesian coordinates, m/s
$\overline{V}$ = mean velocity in y direction, Cartesian coordinates, m/s
x = distance/coordinate in flow direction, m
y = distance/coordinate perpendicular to the wall, m
y^+ = dimensionless distance perpendicular to the wall, $y^+=yu^*/\nu$

Greek letters

Γ = diffusion coefficient, m^2/s
ϵ = turbulent kinetic energy dissipation rate, m^2/s^3
ϵ^+ = dimensionless turbulent kinetic energy dissipation rate, $\epsilon^+=\nu\epsilon/(u^*)^4$
$\tilde{\epsilon}$ = $\epsilon-D$
κ = Von Karmans constant
ν = kinematic viscosity, m^2/s
ν_t = turbulent viscosity, m^2/s
ρ = density, kg/m^3
σ = molecular Schmidt number, $\sigma=\nu/\mathfrak{D}$
σ_ϵ = turbulent Schmidt number for ϵ
σ_k = turbulent Schmidt number for k
τ^+ = dimensionless total shear stress
τ_c = coincidence time interval, s
τ_{tur} = turbulent flow of momentum, kg/m·s
ϕ = dependent variable

Subscript

w = wall value

Literature Cited

Chien, K.-Y., "Predictions of Channel and Boundary Layer Flows with a Low-Reynolds-Number Two-Equation Model of Turbulence," AIAA Paper No. 80-0134 (1980).

Clark, J. A., "A Study of Incompressible Turbulent Boundary Layers in Channel Flow," *ASME J. Basic Eng.*, **90**, 455 (1968).

Dean, R. B., "Reynolds Number Dependence of Skin Friction and Other Bulk Flow Variables in Two-Dimensional Rectangular Duct Flow," *ASME J. Fluids Eng.*, **100**, 215 (1978).

Eckelmann, H., "The Structure of the Viscous Sublayer and the Adjacent Wall Region in a Turbulent Channel," *J. Fluid Mech.*, **65**, Part 3, 439 (1974).

Hanjalic', K., "Practical Predictions by Two-Equation and Other Fast Methods—Twenty Years of Experience," *Proc. from Zoran P. Zaric Memorial Int. Seminar on Near-Wall Turbulence*, Dubrovnik, Yugoslavia (May 16–20, 1988).

Hanson, S., "Broadening of the Measured Frequency Spectrum in a Differential Laser Anemometer due to Interference Plane Gradients," *J. Phys. D: Appl. Phys.*, **6**, 164 (1973).

Hinze, J. O., *Turbulence*, 2nd ed., McGraw-Hill, New York (1975).

Johansson, T. G., and R. I. Karlsson, "LDV Measurements of Higher Order Moments of Velocity Fluctuations in a Turbulent Boundary Layer," *Laser Anemometry in Fluid Mechanics*, Vol. 3, R. J. Adrian, T. Asanuma, F. Durst, F. G. Durão, and J. H. Whitelaw, eds., *Int. Symp. on Applications of Laser Anemometry to Fluid Measurements*, Lisbon, Portugal (1988a).

Johansson, T. G., "An Experimental Study of the Structure of a Flat Plate Turbulent Boundary Layer, Using Laser-Doppler Velocimetry," PhD Thesis, Chalmers Univ. of Technology, Gothenburg, Sweden (1988b).

Jones, W. P., and B. E. Launder, "The Prediction of Laminarization with a Two-Equation Model of Turbulence," *Int. J. Heat Mass Transfer*, **15**, 301 (1972).

Jones, W. P., and B. E. Launder, "The Calculation of Low-Reynolds-Number Phenomena with a Two-Equation Model of Turbulence," *Int. J. Heat Mass Transfer*, **16**, 1119 (1973).

Karlsson, R. I., J. Eriksson, and J. Persson, "LDV Measurements in a Plane Wall Jet in a Large Enclosure," *Int. Symp. Applications of Laser Techniques to Fluid Mechanics*, Lisbon (July 20–23, 1992).

Kim, J., P. Moin, and R. Moser, "Turbulence Statistics in Fully Developed Channel Flow at Low Reynolds Number," *J. Fluid Mech.*, **177**, 133 (1987).

Kreplin, H.-P., and H. Eckelmann, "Behaviour of the Three Fluctuating Velocity Components in the Wall Region of a Turbulent Channel Flow," *Phys. Fluids*, **22**, 1233 (1979).

Laufer, J., "Investigations of Turbulent Flow in a Two-Dimensional Channel," *NACA Rept.*, 1053 (1951).

Lam, C. K. G., and K. Bremhorst, "A Modified Form of the k-ϵ Model for Predicting Wall Turbulence," *ASME J. Fluids Eng.*, **103**, 456 (1981).

Mizushina, T., F. Ogino, Y. Oka, and H. Fukuda, "Turbulent Heat and Mass Transfer Between Wall and Fluid Streams of Large Prandtl and Schmidt Numbers," *Int. J. Heat Mass Transfer*, **14**, 1705 (1971).

Monin, A. S., and A. M. Yaglom, *Statistical Fluid Mechanics*, English ed., Rev., MIT Press, Cambridge, MA (1975).

Nagano, Y., and M. Hisida, "Improved Form of the k-ϵ Model for Wall Turbulent Shear Flows," *ASME J. Fluids Eng.*, **109**, 156 (1987).

Nallasamy, M., "Turbulence Models and Their Applications to the Prediction of Internal Flows: a Review," *Computers & Fluids*, **15**(2), 151 (1987).

Nishino, K., and N. Kasagi, "Turbulence Statistics Measurements in a Two-Dimensional Channel Flow Using a Three-Dimensional Particle Tracking Velocimeter," *Proc. Symp. on Turbulent Shear Flows*, Stanford Univ. (Aug. 21–23, 1989).

Patankar, S. V., *Numerical Heat Transfer and Fluid Flow*, Hemisphere, Washington, DC (1980).

Patel, V. C., W. Rodi, and G. Scheuerer, "Turbulence Models for Near-Wall and Low Reynolds Number Flows: a Review," *AIAA J.*, **23**(9), 1308 (1985).

Rodi, W., "Turbulence Models and Their Application in Hydraulics—State of the Art," Int. Ass. Hydraulics Research, Div. of Experimental and Mathematical Fluid Dynamics, Delft, The Netherlands (1980).

Rosén, C., "Turbulent High-Schmidt-Number Mass Transfer in the Concentration Polarization Boundary Layer over Ultrafiltration Membranes," PhD Thesis, Lund Institute of Technology, Lund, Sweden (1992).

Shaw, D. A., and T. J. Hanratty, "Turbulent Mass Transfer Rates to a Wall for Large Schmidt Numbers," *AIChE J.*, **23**(1), 28 (1977).

Spalding, D. B., "A Single Formula for the Law of the Wall," *ASME J., Appl. Mechanics*, **28**, 455 (1961).

Teenekes, H., and J. L. Lumley, *A First Course in Turbulence*, MIT Press (1972).

Wei, T., and W. W. Willmarth, "Reynolds-Number Effects on the Structure of Turbulent Channel Flow," *J. Fluid Mech.*, **204**, 57 (1989).

Manuscript received July 27, 1992, and revision received Apr. 26, 1993.